



HAL
open science

Dynamics of localized extreme heatwaves in the mid-latitude atmosphere: A conceptual examination

Masoud Rostami, Luca Severino, Stefan Petri, Saeed Hariri

► **To cite this version:**

Masoud Rostami, Luca Severino, Stefan Petri, Saeed Hariri. Dynamics of localized extreme heatwaves in the mid-latitude atmosphere: A conceptual examination. *Atmospheric Science Letters*, 2023, 10.1002/asl.1188 . hal-04190702

HAL Id: hal-04190702

<https://enpc.hal.science/hal-04190702>

Submitted on 29 Aug 2023

HAL is a multi-disciplinary open access archive for the deposit and dissemination of scientific research documents, whether they are published or not. The documents may come from teaching and research institutions in France or abroad, or from public or private research centers.

L'archive ouverte pluridisciplinaire **HAL**, est destinée au dépôt et à la diffusion de documents scientifiques de niveau recherche, publiés ou non, émanant des établissements d'enseignement et de recherche français ou étrangers, des laboratoires publics ou privés.

Dynamics of localized extreme heatwaves in the mid-latitude atmosphere: A conceptual examination

Masoud Rostami^{1,2}  | Luca Severino^{1,3} | Stefan Petri¹  | Saeed Hariri^{4,5}

¹Potsdam Institute for Climate Impact Research (PIK), RD1, Member of the Leibniz Association, Potsdam, Germany

²Laboratoire de Météorologie Dynamique (LMD), Sorbonne University (SU), Ecole Normale Supérieure (ENS), Paris, France

³Department of Environmental Systems Science, ETH Zurich, Zurich, Switzerland

⁴Physical Oceanography and Instrumentation Department, Leibniz Institute for Baltic Sea Research Warnemünde (IOW), Rostock, Germany

⁵Center for Environmental Prediction Rutgers, The State University of New Jersey, New Brunswick, New Jersey, USA

Correspondence

Masoud Rostami, Potsdam Institute for Climate Impact Research (PIK), RD1, Member of the Leibniz Association, Potsdam, Germany.

Email: rostami@pik-potsdam.de; masoud.rostami@lmd.ipsl.fr

Funding information

H & M Foundation, Grant/Award Number: 20A048

Abstract

This study investigates the adjustment of large-scale localized buoyancy anomalies in mid-latitude regions and the nonlinear evolution of associated condensation patterns in both adiabatic and moist-convective environments. This investigation is carried out utilizing the two-layer idealized moist-convective thermal rotating shallow water (mcTRSW) model. Our investigation reveals that the presence of a circular positive potential temperature anomaly in the lower layer initiates an anticyclonic high-pressure rotation, accompanied by a negative buoyancy anomaly in the upper layer, resulting in an anisotropic northeast–southwest tilted circulation of heat flux. The evolution of eddy heat fluxes, such as poleward heat flux, energy, and meridional elongation of the buoyancy field, heavily depends on the perturbation's strength, size, and vertical structure. The heatwave initiates atmospheric instability, leading to precipitation systems such as rain bands and asymmetric latent heat release due to moist convection in a diabatic environment. This creates a comma cloud pattern in the upper troposphere and a comma-shaped buoyancy anomaly in the lower layer, accompanied by the emission of inertia gravity waves. The southern and eastern sectors of the buoyancy anomaly show an upward flux, generating a stronger cross-equatorial flow and inertia-gravity waves in a southward and eastward direction. Furthermore, the simulations reveal a similar asymmetric pattern of total condensed liquid water content distribution, accompanied by the intensification of moist convection as rain bands. This intensification is more pronounced in barotropic structures than in baroclinic configurations with stagnant upper layers. This study highlights the importance of considering moist convection and its effects on atmospheric and oceanic flows in mid-latitude regions, as well as the role of buoyancy anomalies in generating heatwaves and precipitation patterns.

KEYWORDS

Aeolus 2.0, geostrophic adjustment, heatwaves, moist-convection, thermal rotating shallow water (TRSW) model

This is an open access article under the terms of the [Creative Commons Attribution](https://creativecommons.org/licenses/by/4.0/) License, which permits use, distribution and reproduction in any medium, provided the original work is properly cited.

© 2023 The Authors. *Atmospheric Science Letters* published by John Wiley & Sons Ltd on behalf of Royal Meteorological Society.

1 | INTRODUCTION

Heatwaves are becoming increasingly frequent and severe worldwide, with mid-latitude regions being particularly affected. Recent examples include heatwaves observed in North America, Europe, and Asia (Diffenbaugh & Ashfaq, 2010; Hansen et al., 2012; Perkins et al., 2012). The origins of heatwaves can be attributed to various physical drivers that fall into two primary categories: atmospheric drivers, which encompass processes related to moisture and radiation, and surface drivers. Additionally, the drivers from both the atmosphere and surface can interact and produce combined nonlinear effects, as discussed in previous studies (for a comprehensive review of heatwave drivers, see Horton et al. (2016), Miralles et al. (2019)). It is important to emphasize that, in the context of this study, the term “heatwaves” refers to the intricate progression and dynamic evolution of extensive, localized positive buoyancy anomalies. These anomalies originate from elevated potential temperatures, emerging in the absence of simultaneous background zonal fluid motion, through “conceptual” examinations, which involve the use of an idealized model (also refer to Section 2). Such distinct anomalies demonstrate the ability to persist over an extended period spanning multiple days. The association between warm extremes and persistent high-pressure anomalies, commonly referred to as blocking-like circulation patterns, has been frequently documented in the scientific literature (Cassou et al., 2005; Meehl & Tebaldi, 2004; Stefanon et al., 2012; Xoplaki et al., 2003). These blocking patterns typically manifest as ridges or cut-off highs in the geopotential height contours of the upper troposphere. However, the underlying causal mechanisms linking these phenomena remain inadequately explored, with limited explicit ridge simulations or conceptual frameworks available. To address this knowledge gap, the present study endeavors to investigate the potential influence of surface warm extremes on the occurrence of upper tropospheric atmospheric ridges. Our research uncovers that upper tropospheric atmospheric ridges can manifest concurrently with surface warm localized anomalies. This concurrent development is attributed to the heating effects near the Earth’s surface, which induce the formation of a thermal low-pressure system and a cyclonic circulation pattern in the lower atmosphere, countering the prevailing upper-level anticyclone. The simultaneous occurrence of these phenomena is corroborated by observational studies, such as the comprehensive investigation conducted by Pfahl and Wernli (2012). It is important to note that a universally accepted theory encompassing all aspects of heatwaves is currently lacking. The primary objective of our study is not to replicate real heatwaves precisely but rather to simulate the concept of buoyancy

anomalies in a robust manner to capture their fundamental characteristics.

In a “dry” environment, the establishment of geostrophic balance involves the development of a horizontal temperature gradient due to a localized heat disturbance (Holton, 2004). The term “dry” signifies an adiabatic process in which no condensation or phase transition of water vapor occurs, thereby ensuring the conservation of total energy. However, the nonadiabatic adjustment process is also influenced by the vertical structure of the atmosphere, air mass stability, and the presence of moist convection and wind shear. Moist convection has a significant impact on the dynamic response of the mid-latitude atmosphere, affecting weather and climate prediction and dynamics. To accurately model the interactions between moist convection and geostrophic adjustment, sophisticated numerical modeling techniques are necessary, along with a comprehensive understanding of the fundamental physical processes involved.

The rotating shallow water (RSW) model is a widely used tool for studying atmospheric and oceanic flows in mid-latitude regions. It is based on the integration of atmospheric primitive equations using pseudo-height isobaric vertical coordinates, which allows it to capture important features of large-scale fluid dynamics such as jet streams and Rossby waves (Zeitlin, 2018). However, the classical RSW model has some limitations. In particular, it neglects the effects of horizontal gradients of potential temperature and moist convection, which can be significant in certain atmospheric and oceanic flows. These effects arise from the interaction between temperature and water vapor content, and can lead to the formation of clouds, precipitation, and other atmospheric features. To overcome these limitations, researchers have developed modified versions of the RSW model that take these effects into account. One such model is the moist-convective thermal rotating shallow water (mcTRSW) model (cf., Rostami et al., 2022). The mcTRSW model incorporates the effects of horizontal gradients of potential temperature and moist convection, resulting in more accurate simulations of atmospheric currents than those produced by classical RSW models. Given these advantages, the mcTRSW model is a suitable choice for investigating the fully nonlinear adjustment of large-scale positive buoyancy anomalies in a moist-convective environment. Positive buoyancy anomalies are regions where air parcels are warmer and less dense than their surroundings and thus tend to rise. Understanding the dynamics of such anomalies is important for predicting the behavior of the atmosphere in various weather and climate conditions. The mcTRSW model can help shed light on these processes and provide insights into the complex interactions between temperature, water vapor content, and large-scale atmospheric dynamics.

Several studies have explored the atmospheric responses to sea surface temperature (SST) anomalies, including moisture, using complex models, as comprehensively reviewed by (Zhou, 2019). However, within the realm of conceptual models, although extensive research has been conducted on simplified models such as one-dimensional models (e.g., Blumen, 1972; Gill, 1976, 1982) and linearized models specifically designed for “dry” environments (e.g., Lim & Chang, 1981; Matsuda & Takayamal, 1989), the comprehensive examination of fully nonlinear adjustments of large-scale positive buoyancy anomalies using a multi-layer moist-convective thermal rotating shallow water (TRSW) conceptual model or other similar conceptual models are still relatively limited in the existing literature. This study aims to fill this research gap by investigating the dynamic behavior of such adjustments and their potential implications for weather and climate prediction.

2 | MODEL DESCRIPTION AND SETUP OF NUMERICAL EXPERIMENTS

The model utilized in this study is supported by a theoretical foundation with a historical record for the incorporation of moist convection. The model is based on the mcRSW model, which has already incorporated phase transitions of water vapor and the related latent heat release (Bouchut et al., 2009; Lambaerts et al., 2012; Lambaerts, Lapeyre, & Zeitlin, 2011; Lambaerts, Lapeyre, Zeitlin, & Bouchut, 2011). The evolution of the vertically averaged humidity and the corresponding effects of condensation and latent heat release on the air column are defined in the mcRSW model in a simple and consistent way, following the seminal ideas of Gill (1982). The mcRSW model has been continuously improved, and the applied version in this study includes additional features such as precipitable water, vaporization, and precipitation, as proposed by Rostami and Zeitlin (2018). This improved model has been used in numerous studies to investigate the effects of moist convection on the dynamics of large-scale Earth and planetary jets and vortices (Lahaye & Zeitlin, 2016; Lambaerts et al., 2012; Rostami et al., 2017; Rostami & Zeitlin, 2017; Rostami & Zeitlin, 2019a, 2019b, 2020, 2022a).

The simplified two-layer mcTRSW model is characterized by the set of equations outlined by Rostami et al. (2022) as below:

$$\frac{d_1 \mathbf{v}_1}{dt} + f \hat{\mathbf{z}} \times \mathbf{v}_1 = -\frac{1}{2} h_1 \nabla b_1 - b_1 \nabla (h_1 + h_2), \quad (1a)$$

$$\begin{aligned} \frac{d_2 \mathbf{v}_2}{dt} + f \hat{\mathbf{z}} \times \mathbf{v}_2 = & -\frac{1}{2} h_2 \nabla b_2 - \nabla (h_1 b_1) - b_2 \nabla (h_b + h_2) \\ & - \frac{1-\gamma}{b_2 h_2} (\mathbf{v}_2 - \mathbf{v}_1) (C), \end{aligned} \quad (1b)$$

$$\partial_t h_1 + \nabla \cdot (h_1 \mathbf{v}_1) = \frac{1-\gamma}{b_1} (-C) + (1-\gamma^*) \frac{h_1 - (B_1/b_1) H_1}{\tau_r}, \quad (1c)$$

$$\partial_t h_2 + \nabla \cdot (h_2 \mathbf{v}_2) = \frac{1}{b_2} (+C) + (1-\gamma^*) \frac{h_2 - (B_2/b_2) H_2}{\tau_r}, \quad (1d)$$

$$\partial_t b_1 + \mathbf{v}_1 \cdot \nabla b_1 = \frac{1}{h_1} (+C) - \frac{b_1 - (H_1/h_1) B_1}{\tau_r}, \quad (1e)$$

$$\partial_t b_2 + \mathbf{v}_2 \cdot \nabla b_2 = \frac{1}{h_2} (-C) - \frac{b_2 - (H_2/h_2) B_2}{\tau_r}, \quad (1f)$$

$$\partial_t q_1 + \nabla \cdot (q_1 \mathbf{v}_1) = E_s - C, \quad (1g)$$

$$\partial_t q_2 + \nabla \cdot (q_2 \mathbf{v}_1) = C. \quad (1h)$$

The Lagrangian derivative is given by $d_i/dt = \partial/\partial t + \mathbf{v}_i \cdot \nabla$, where \mathbf{v}_i represents the vertically-averaged horizontal velocity in layer i , and ∇ denotes the two-dimensional gradient operator. The thickness of each layer is denoted by h_i and numbered from the bottom to the top of the domain. The parameters H_i and B_i represent the thickness and buoyancy at rest state, respectively. The layer-averaged buoyancy variable, b_i , is defined as $g \bar{\theta}_i / \theta_s$, where $\bar{\theta}_i$ is the vertically-averaged horizontal potential temperature in layer i . The potential temperature (θ) in atmospheric dynamics refers to a thermodynamic variable that characterizes the temperature of a parcel of air in a way that accounts for the influence of pressure changes. It is defined as the temperature that a parcel of dry air would attain if adiabatically brought to a reference pressure level, typically chosen as the surface pressure. It serves as a conservative quantity that remains constant for a dry adiabatic process and can be expressed as: $\theta = T(P_s/P)^{\mathcal{R}/C_p}$, where T is the actual temperature of the parcel, P_s is the reference pressure level, P is the pressure of the parcel, \mathcal{R} is the specific gas constant for dry air, and C_p is the specific heat capacity at constant pressure. g is the acceleration due to gravity, and θ_s is the potential temperature at the lowermost layer, typically at the surface. Additionally, C and E_s denote the condensed liquid water content (CLWC) in the lower layer and the bulk formula for surface evaporation, respectively. The parameters γ and γ^*

represent the contribution of condensation, due to latent heat release, and Newtonian cooling to the bulk entropy of the air column, which can vary from layer to layer. The parameter f denotes the Coriolis parameter, while $\hat{\mathbf{z}}$ represents a unit vector in the vertical direction.

Note that in Equations (1), we assume $b_i \gg q_i/h_i$ to simplify the equations, where q_i represents the specific humidity or water vapor content integrated over the air column. However, the magnitude of q_i/h_i relative to other terms, such as b_i , is not negligible. Therefore, we include q_i/h_i in the model to accurately capture the effect of water vapor. Scaling and parameters are the same as (Rostami et al., 2022). The corresponding equations of precipitable water, downward draft, Newtonian viscosity, and vaporization used in the model but not presented in Equations (1) follow Rostami and Zeitlin (2018).

We parameterize CLWC using the Betts–Miller method (Betts & Miller, 1986) and surface evaporation, E_s , using a standard approach for ocean–atmosphere exchanges (Katsaros, 2001). The numerical methods used in the experiments follow the Dedalus algorithm, which utilizes spin-weighted spherical harmonics (Lecoanet et al., 2019; Vasil et al., 2019).

The thermogeostrophic balance relations in an adiabatic environment can be expressed as:

$$f_0 \hat{\mathbf{z}} \times \mathbf{v}_1^{(0)} = -\frac{1}{2} h_1^{(0)} \nabla b_1^{(0)} - b_1^{(0)} \nabla (h_1^{(0)} + h_2^{(0)}), \quad (2a)$$

$$f_0 \hat{\mathbf{z}} \times \mathbf{v}_2^{(0)} = -h_1^{(0)} \nabla b_1^{(0)} - \frac{1}{2} h_2^{(0)} \nabla b_2^{(0)} - b_1^{(0)} \nabla h_1^{(0)} - b_2^{(0)} \nabla h_2^{(0)}. \quad (2b)$$

Here, the superscript (0) denotes the leading-order variables and f_0 represents the Coriolis parameter at a reference latitude.

To clarify the interplay between positive buoyancy anomalies or positive gradients of potential temperature and negative pressure anomalies, we present the system of evolution equations for a two-layer TRSW model in a “dry” environment. The model equations can be expressed as follows:

$$(\partial_t + \mathbf{v}_1 \cdot \nabla) \mathbf{v}_1 + f \hat{\mathbf{z}} \times \mathbf{v}_1 = -\langle \nabla p_1 \rangle, \quad (3a)$$

$$(\partial_t + \mathbf{v}_2 \cdot \nabla) \mathbf{v}_2 + f \hat{\mathbf{z}} \times \mathbf{v}_2 = -\langle \nabla p_2 \rangle, \quad (3b)$$

$$\partial_t h_1 + \nabla \cdot (h_1 \mathbf{v}_1) = 0, \quad (3c)$$

$$\partial_t h_2 + \nabla \cdot (h_2 \mathbf{v}_2) = 0, \quad (3d)$$

$$\partial_t b_1 + \mathbf{v}_1 \cdot \nabla b_1 = 0, \quad (3e)$$

$$\partial_t b_2 + \mathbf{v}_2 \cdot \nabla b_2 = 0. \quad (3f)$$

In the above equations, $\mathbf{v}_i = (u_i, v_i)$ represents the horizontal velocity, and $\langle \nabla p_i \rangle = \nabla \tilde{p}_i - \tilde{h}_i \nabla b_i$ represents the vertically-averaged horizontal gradient of the pressure field. The indices $i=1,2$ correspond to the lower and upper layers, respectively. The expressions for \tilde{p}_1 , \tilde{p}_2 , \tilde{h}_1 , and \tilde{h}_2 are defined as follows: $\tilde{p}_1 = (h_b + h_1 + h_2) b_1$, $\tilde{p}_2 = h_1 b_1 + (h_b + h_2) b_2$, $\tilde{h}_1 = h_b + (1/2) h_1 + h_2$, and $\tilde{h}_2 = h_b + (1/2) h_2$. The quantities $\langle \nabla p_1 \rangle$ and $\langle \nabla p_2 \rangle$ can be expressed as $(1/2) h_1 \nabla b_1 + b_1 \nabla (h_b + h_1 + h_2)$ and $\nabla (h_1 b_1) + (1/2) h_2 \nabla b_2 + b_2 \nabla (h_b + h_2)$, respectively. It is important to note that the vector fields of $\langle \nabla p_i \rangle$ do not correspond to the gradient of a scalar. The evolution Equations (3) are satisfied within a defined horizontal domain \mathcal{D} . The first boundary condition is characterized by the absence of normal flux, expressed as:

$$\hat{\mathbf{n}} \cdot h_i \mathbf{v}_i = 0, \quad x \in \partial \mathcal{D}, \quad (4)$$

where $\hat{\mathbf{n}}$ represents the outward unit vector. A suitable Hamiltonian, which serves as a comprehensive measure of the total energy in the system described by Equation (3), encompassing both kinetic energy and gravitational potential energy, can be defined as follows:

$$\mathcal{H} = \int_{\mathcal{D}} d^2x \left[h_1 \left(\frac{1}{2} \mathbf{v}_1^2 + \tilde{h}_1 b_1 \right) + h_2 \left(\frac{1}{2} \mathbf{v}_2^2 + \tilde{h}_2 b_2 \right) \right]. \quad (5)$$

The functional derivatives of the Hamiltonian \mathcal{H} can be obtained as follows:

$$\frac{\delta \mathcal{H}}{\delta \mathbf{v}_k} = h_k \mathbf{v}_k, \quad \frac{\delta \mathcal{H}}{\delta h_k} = \zeta_k, \quad \frac{\delta \mathcal{H}}{\delta b_k} = h_k \tilde{h}_k. \quad (6)$$

Here, $\zeta_i = \tilde{p}_i + (1/2) \mathbf{v}_i^2$ represents the Bernoulli head in each layer. It is important to note that, in general, $\partial \tilde{h}_k / \partial h_k$ does not vanish when calculating $\delta \mathcal{H} / \delta h_k$. The total mechanical energy of the system, as defined in Equation (5), remains conserved, ensuring the boundedness of the system's free evolution. The term $d^2x (1/2) h_i \mathbf{v}_i^2$ represents the kinetic energy associated with an elementary fluid column in the i th layer, calculated under the Boussinesq approximation. Furthermore, the height of the elementary column above the reference level $z=0$ in the i th layer is denoted as \tilde{h}_i , and its absolute potential energy is given by $d^2x h_i \tilde{h}_i b_i$. This conservation applies to the sum of kinetic energy and potential energy of the active layers, relative to them being filled with stable stratified layers with potential temperatures $\theta_2 > \theta_1$. For a detailed proof of this conservation law, refer to Ripa (1993).

This study employs numerical simulations to investigate the dissipation of a large-scale, localized positive buoyancy anomaly in mid-latitudes under both “dry” and moist-convective conditions. To isolate the specific impact of the initial potential temperature disturbance on the atmospheric response and exclude any potential influence from background zonal velocity, we omitted the inclusion of background flow and topography in our conceptual experiments. This is due to the high sensitivity of the mid-latitude atmospheric response to lower buoyancy anomalies, particularly over the ocean, to the background state (Thomson & Vallis, 2018). By adopting this approach, we effectively isolate and elucidate the intrinsic processes governing the temporal evolution of the buoyancy anomaly, facilitating a direct and focused investigation into its intricate dynamics and dissipation mechanisms with a high degree of clarity and confidence. The initial buoyancy disturbance is expressed by a simplified circular α -Gaussian equation (cf., Rostami & Zeitlin, 2017), which is constrained not only in latitude but also in longitude. The equation is given by:

$$b_i = \epsilon H_i \sqrt{2e} \frac{2^{1/\sigma}}{\sigma} \Gamma\left(\frac{1}{\sigma} + \frac{1}{2}\right) G\left(\frac{r^\sigma}{2}, \frac{1}{\sigma} + \frac{1}{2}\right), \quad i = 1, 2, \quad H_1 = H_2 = 0.5. \quad (7)$$

Here, b_i represents the non-dimensional buoyancy anomaly for layer i , ϵ is the maximum amplitude of the anomaly, σ is a parameter that determines the width of the anomaly and is set to 4, and r is the spherical distance from the center of the anomaly to the location of interest, calculated using the Haversine formula as $\mathcal{D}(Lat_0, Lon_0, Lat, Lon)$, where $Lat_0 = 40$ and $Lon_0 = 0$. The function $\Gamma(x)$ denotes the Gamma function and $G(r, a)$ is given by $G(r, a) = [1/\Gamma(a)] \int_r^a e^{-t} t^{a-1} dt$. The parameters ϵ and σ determine the amplitude and steepness of the thickness anomaly, respectively, and H_i represents the thickness of each layer. In the barotropic configuration, $b_1 = b_2$, and in the baroclinic case, $b_2 = 0$. The equality in phase of upper and lower-level buoyancy anomalies defines barotropic disturbances with symmetric behavior and horizontal influence. Conversely, the inequality in phase, with an absent or reduced upper-level buoyancy anomaly, characterizes baroclinic disturbances with asymmetry, and the formation of cyclonic and anticyclonic circulation patterns. Two different amplitudes are considered for ϵ : 0.1 for a weak anomaly and 0.3 for a strong anomaly. In a moist-convective environment, the initial distribution of water vapor in the lower layer is chosen to be close to saturation, while the upper layer is far from saturation. This setup ensures

that condensation primarily occurs in the lower layer. The model includes entrainment of CLWC from the lower to upper layer through upward convective flux, as introduced in Rostami and Zeitlin (2022b).

The zonal and meridional scales of the circular α -Gaussian spatial distribution at half-maximum intensity are approximately 32° , which is of the same order of magnitude as the Rossby deformation radius at midlatitudes in a barotropic atmosphere. This suggests that the scale of the initial buoyancy disturbance is comparable to the characteristic scale of the deformation field in the atmosphere, and thus it can potentially induce Rossby waves and trigger other dynamical processes in the atmosphere.

3 | RESULTS

In the early stages of the positive buoyancy anomaly adjustment process, a nearly isotropic inflow towards the center of the anomaly is observed. This is because the anomaly initially creates a region of low pressure that attracts surrounding air masses from all directions. However, as the anomaly develops, wind directions begin to deviate from the center, primarily due to the Coriolis force, which results from the Earth's rotation. In the Northern Hemisphere, the Coriolis force deflects the direction of air masses to the right, while in the Southern Hemisphere, it deflects them to the left. As a result, asymmetric convergent zones develop, where air masses converge toward the center of the anomaly from specific directions, leading to the development of asymmetry in the CLWC and divergence fields, as illustrated in Figures 1, 2. These convergent zones influence the distribution of moist-convective fronts, leading to the formation of precipitable water patterns, such as spiral rain bands, around the anomaly. These patterns result from the interaction between the converging air masses and the surrounding environment, including the beta effect. Specifically, the beta effect describes how the Coriolis force increases with latitude in a rotating system with a varying angular velocity, such as the atmosphere. Additionally, the asymmetric flow generated by the buoyancy anomaly produces perturbations in the large-scale circulation that can affect the development and evolution of other weather systems in the region, such as cyclones and anticyclones. The evolution of both the lower- and upper-layer buoyancy anomaly and fronts are primarily affected by geostrophic and secondarily by ageostrophic circulations. Geostrophic circulations arise from the balance between the Coriolis force and the pressure gradient force, while ageostrophic circulations result from the imbalance between these forces. The interaction between these circulations can result in the formation of

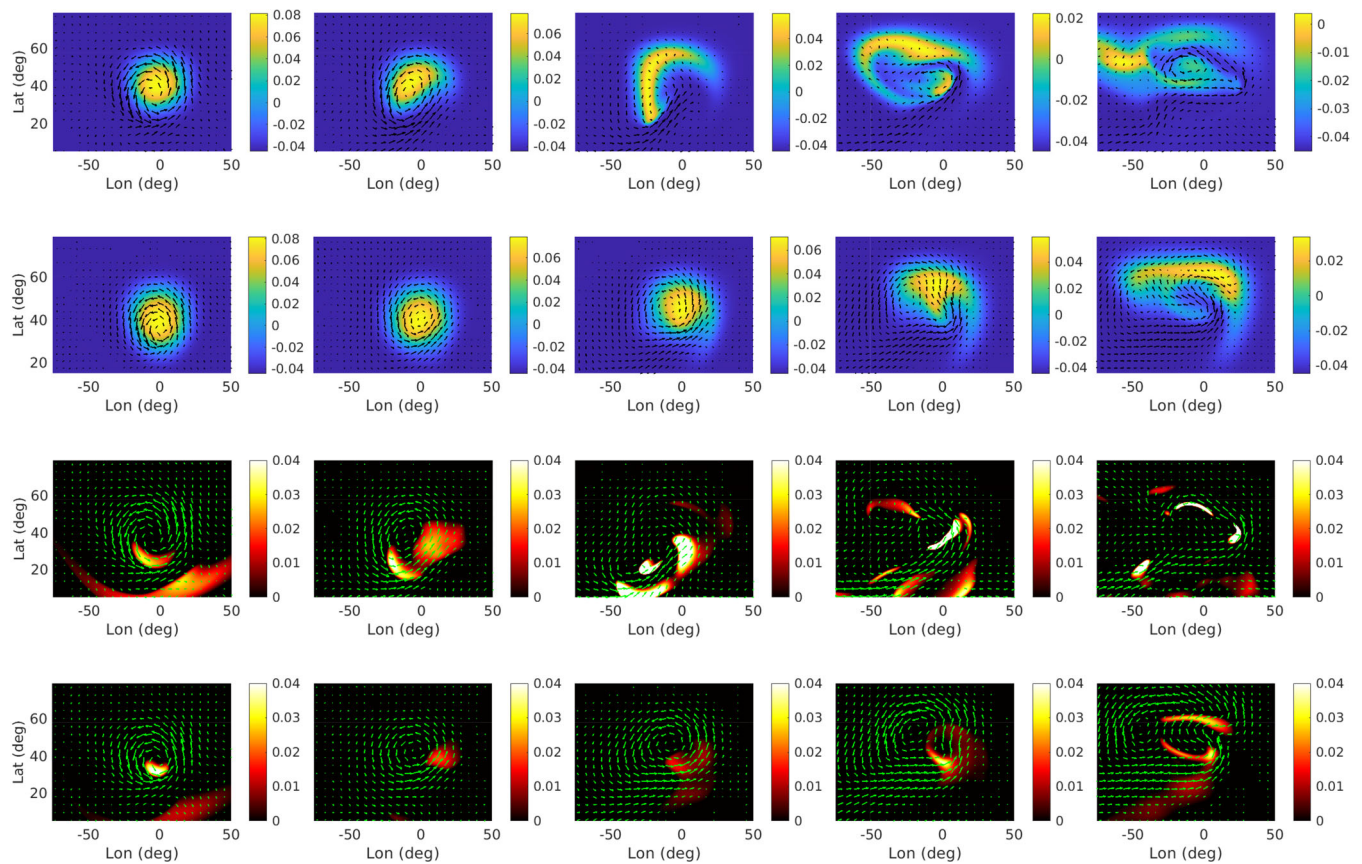


FIGURE 1 The evolution of buoyancy perturbations, CLWC (represented in colors) in the lower troposphere, and the corresponding velocity field (represented by arrows) during midlatitude adjustment in a moist-convective environment. The first and second rows show the results for barotropic and baroclinic configurations, respectively. The third and fourth rows show the evolution of CLWC (represented in colors) in the lower layer and the corresponding baroclinic velocity field (represented by arrows) for barotropic and baroclinic configurations. The panels in each row display the field evolution at times of 6, 13, 26, 43, and 65 days, arranged from left to right. The colorbars are adjusted panel-wise for improved visibility.

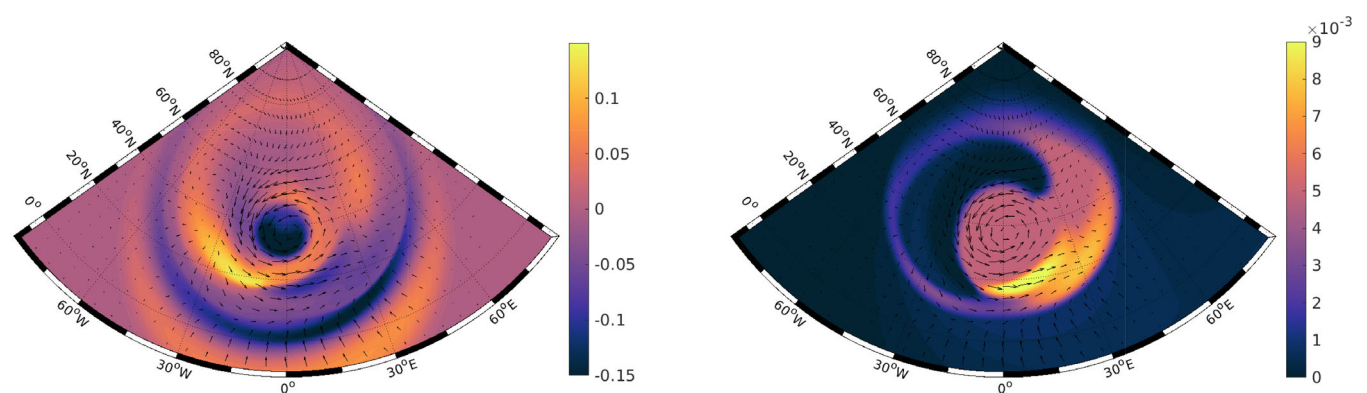


FIGURE 2 The left panel shows snapshots of the divergence field, while the right panel displays precipitable water in the lower layer, both during the midlatitude adjustment of a barotropic configuration in a moist-convective environment. The corresponding velocity field is represented by arrows. These snapshots were taken on the fifth day of simulation.

frontal zones, which separate air masses of different temperatures and densities, contributing to the development of precipitation systems and other weather phenomena. Our

findings suggest that the heatwave triggers the formation of mesoscale convective systems, which can produce heavy rainfall and corresponding rain bands, especially in the

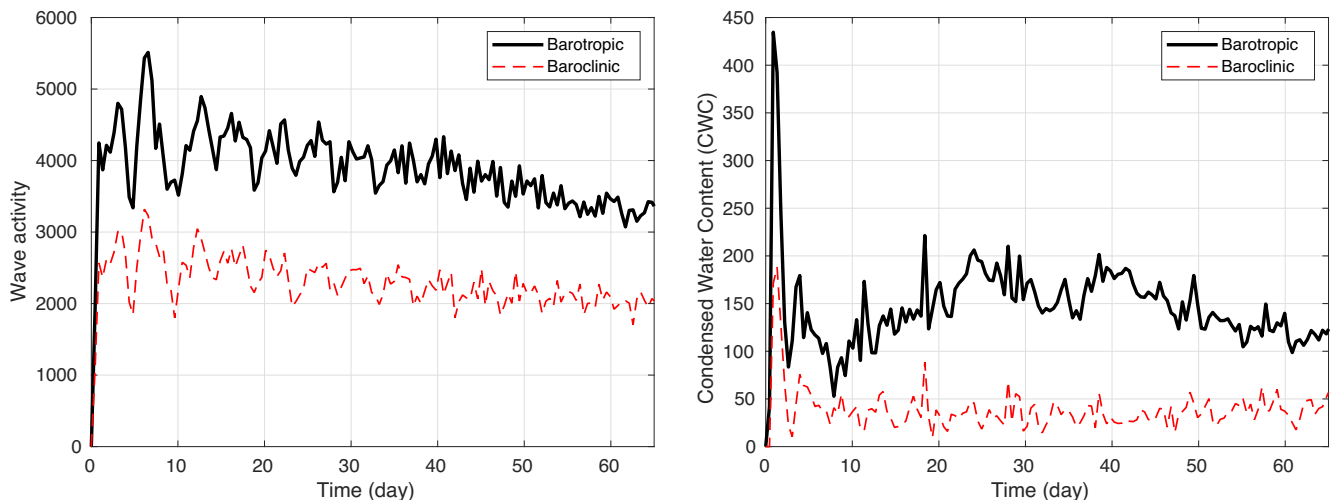


FIGURE 3 The left panel displays the evolution of inertia-gravity wave activity, while the right panel shows the condensed liquid water content (CLWC) in the lower layer. Both panels show the results for the barotropic and baroclinic configurations, where the upper layer is stagnant, during midlatitude adjustment caused by a strong positive buoyancy anomaly at the initial time.

southern and western sectors near the buoyancy anomaly (Figure 1). The formation of mesoscale convective systems is influenced by various factors such as the strength and size of the buoyancy anomaly, the vertical structure of the atmosphere, and the presence of other environmental factors such as wind shear and moisture content.

During the initial stages of midlatitude adjustment, there is an abrupt emission of inertia-gravity waves, which can be observed in inertia-gravity wave activity diagrams (Figure 3). In this context, inertia-gravity wave activity is determined by integrating the divergence of the velocity field. In a moist-convective environment, the southern sectors exhibit a heightened occurrence of vigorous inertia-gravity waves in comparison to the northern regions. The convective activity linked to the buoyancy anomaly engenders more robust and coherent regions of condensation that impact the layer thicknesses (h_1, h_2) and buoyancy variables (b_1, b_2) as described by Equation (1), thereby amplifying the wave generation in those directions. When a disturbance with a large amplitude is introduced in the mid-latitudes, the inertia-gravity waves produced during the geostrophic adjustment process disperse equatorward and dissipate over the tropical region. These waves play an essential role in the redistribution of heat and momentum within the lower troposphere. The findings of our study indicate that mid-latitude heatwaves can enhance the moisture transport from the ocean to the atmosphere, leading to increased atmospheric moisture content and the potential for increased cloud formation and condensation. The dominance of southward-propagating inertia-gravity waves, along with westward-travelling Rossby waves, is also evident in the spatial distribution of the energy density anomaly depicted in Figure 8.

Intense buoyancy anomalies exert a pivotal influence on the initiation of cyclonic structures (Figure 1). Empirical investigations, notably those conducted within the Atlantic basin, furnish compelling evidence for the conspicuous linkage between explosive cyclogenesis and regions characterized by pronounced SST gradients (Sanders & Gyakum, 1980). The genesis of such surface temperature anomalies can be attributed to diverse factors, including the total surface net radiation, the depletion of soil moisture, or the prevalence of drought conditions, thereby substantially curtailing latent cooling and amplifying surface temperature anomalies (Fischer et al., 2007; Zaitchik et al., 2006).

Within the purview of our inquiry, we ascertain that buoyancy anomalies in the lower troposphere instigate the formation of an upper-tropospheric anticyclonic structure (Figure 4). This finding robustly substantiates the concurrent generation paradigm, whereby cyclonic circulation patterns manifest at lower atmospheric levels concomitantly with anticyclonic circulation patterns at upper atmospheric levels. The manifestation of the Pacific Northwest heatwave in June 2021 provided compelling evidence of the temporal relationship between temperature anomalies and the subsequent intensification of a low-pressure system at sea-level pressure. Notably, 1 week prior to the heatwave's onset on 25 June, temperature anomalies surpassed a threshold of two standard deviations, thereby initiating the process of low-pressure system intensification (White et al., 2023). The phenomenon of enhanced ridging in the (mid-)upper troposphere manifests as an elongated region typified by relatively elevated atmospheric pressure vis-à-vis its environs. This configuration engenders more stable and enduring weather patterns, characterized by predominantly clear and arid

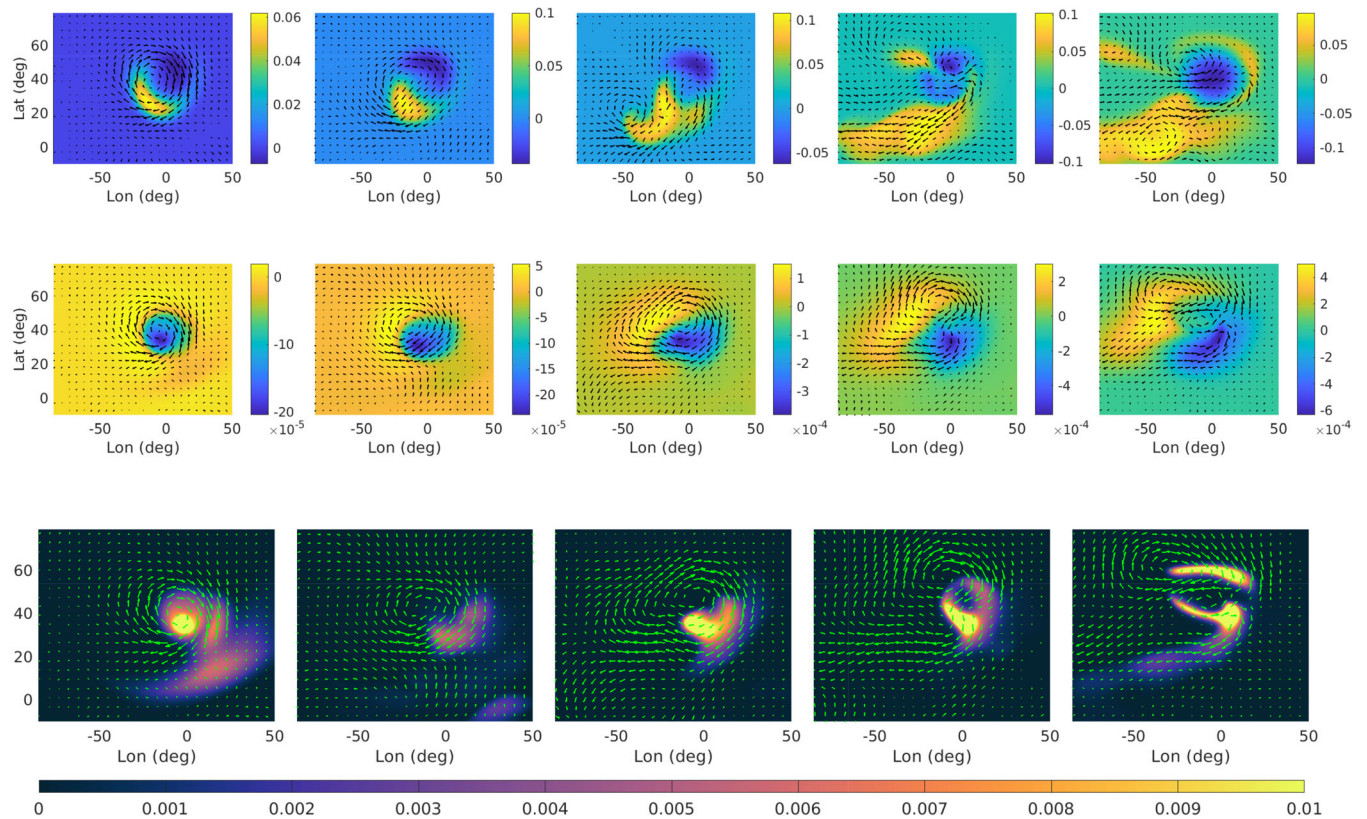


FIGURE 4 The evolution of buoyancy perturbations (represented in color) in the upper troposphere and the corresponding velocity field (represented by arrows) associated with midlatitude adjustment in a moist-convective environment. The first and second rows show the results for the barotropic and baroclinic configurations, respectively. The third row presents the evolution of precipitable water as cloud shields, the formation of a comma pattern, and its entrainment in the upper layer for the baroclinic configuration with a stagnant upper layer. The panels in each row display the field's evolution at different time points, including 6, 13, 26, 43, and 65 days, from left to right. The colorbars are adjusted panel-wise for improved visibility.

conditions, thereby facilitating the advection and entrainment of warm air masses. Notably, during the later stages of the simulation, the primary anticyclone nucleus migrates poleward and gradually engenders secondary vortices (second row of Figure 4). The recurrence of a persistent pattern of mid- to upper-tropospheric anticyclonic circulation and enhanced ridging has been frequently documented in previous observational inquiries (cf., Black et al., 2004; Cassou et al., 2005; Meehl & Tebaldi, 2004; Pfahl & Wernli, 2012; Xoplaki et al., 2003). Therefore, while we acknowledge and respect hypotheses such as the one put forth by Black et al. (2004), which posits that the initial manifestation of extreme temperature anomalies is primarily ascribable to the enduring anticyclonic circulation anomaly, our study unveils the plausibility of an additional causal pathway. Specifically, our findings elucidate that anticyclonic structures can arise concomitantly due to low-level positive potential temperature anomalies. Thus, while not discounting the hypotheses like the one postulated by Black et al. (2004), which posits that the initial manifestation of extreme temperature anomalies is

primarily ascribable to the enduring anticyclonic circulation anomaly, our study unveils the plausibility of an additional causal pathway. Thus, the origin of these anticyclonic structures differs from those created by midlatitude jet streams. It is worth noting that the meandering of mid-latitude jet streams, such as the polar front jet stream, can also contribute to the formation of cyclonic and anticyclonic structures in the atmosphere (Okajima et al., 2021). When a meander or wave in the jet stream becomes stationary or slows down, it can lead to the persistence of high-pressure systems over a specific region, resulting in blocking patterns.

The evolution of precipitable water in the upper troposphere results in the formation of a comma cloud pattern, as seen in Figure 4. This pattern is a result of the interaction between the cyclonic flow in the lower troposphere and the anticyclonic flow in the upper troposphere, creating a distinct comma shape. Observational studies have reported such comma cloud patterns (Carlson, 1980).

Comparative analysis of the barotropic and baroclinic configurations, when coupled with a stagnant upper

layer, reveals that inertia-gravity wave activity is stronger in the barotropic configuration. This is attributed to the resulting temperature gradient, which drives the formation of an anticyclone in the upper troposphere. The anticyclone persists even after the cyclone has dissipated in the lower troposphere. In both configurations, the warm core in the lower troposphere strengthens as the cyclone intensifies, accompanied by the development of a cold core in the upper troposphere. However, the evolution of buoyancy in the upper layer differs between the baroclinic and barotropic scenarios. In the baroclinic case, buoyancy increases towards the northwest, while in the barotropic scenario, buoyancy increases towards the south and southwest (Figure 4). These differences in the evolution of buoyancy between the two configurations have significant implications for the subsequent development and evolution of midlatitude cyclones. Over time, the anticyclone evolves into the upper-level trough and ridge (Figure 4). These numerical results align with the crudest feature of the formation of a cold core in the upper troposphere observed in other studies (e.g., Chang et al., 2019).

As Rossby waves' westward phase velocity reduces with increasing latitude, a disturbance's phase in lower latitudes will precede that in higher latitudes. Therefore, following the development of cyclonic circulation in the lower layer, the northeast-southwest tilt of the buoyancy disturbance, as observed during evolution (Figure 1, second panel at Time = 13 days), appears. It is worth reminding that low-frequency Rossby waves evolve slowly. Subsequently, the isentropic surfaces of both weak and strong buoyancy anomalies develop a comma-shaped structure and are displaced towards the northwest by the beta-gyres. The beta-gyre pattern is significantly

affected by various factors such as the anomaly's strength, the presence of moist convection, and the vertical structure's barotropic or baroclinic nature (refer to Figures 1, 5). Enhanced asymmetry, resulting from beta-gyres, leads to instabilities developing in the system's core and the formation of smaller rotating vortices known as secondary eyewall mesovortices. These mesovortices have been frequently observed in tropical cyclones, as documented in previous studies (e.g., Kossin et al., 2002). The meridional displacement of anomalies increases with buoyancy intensity, and strong northwestward-drifting anomalies eventually veer eastward. Eastward veering is more prominent in barotropic configurations than in baroclinic ones (refer to Figures 1, 5). In an adiabatic environment devoid of moist convection, the dissipation of buoyancy anomalies exhibits a delayed occurrence compared to their counterparts in a moist-convective environment. This temporal discrepancy is demonstrated in Figures 1, 5, which illustrate the evolution of buoyancy anomalies in both moist-convective and dry conditions, respectively.

During the late stages of strong buoyancy anomaly evolution, particularly in barotropic configurations, a breaking process occurs, which can result in the transport of a parallel heat flux towards the north. This complex process is evident in the Hovmöller diagram, which illustrates the anomaly's time evolution as it propagates northward (see Figure 6). The breaking of the anomaly depends on several factors, such as the strength of the anomaly, the presence of moist convection, and the baroclinicity of the vertical structure. In barotropic configurations, the breaking of the anomaly is more pronounced, resulting in a more significant transport of heat towards the north. This breaking process is thought to be related to the development of strong shear zones near the

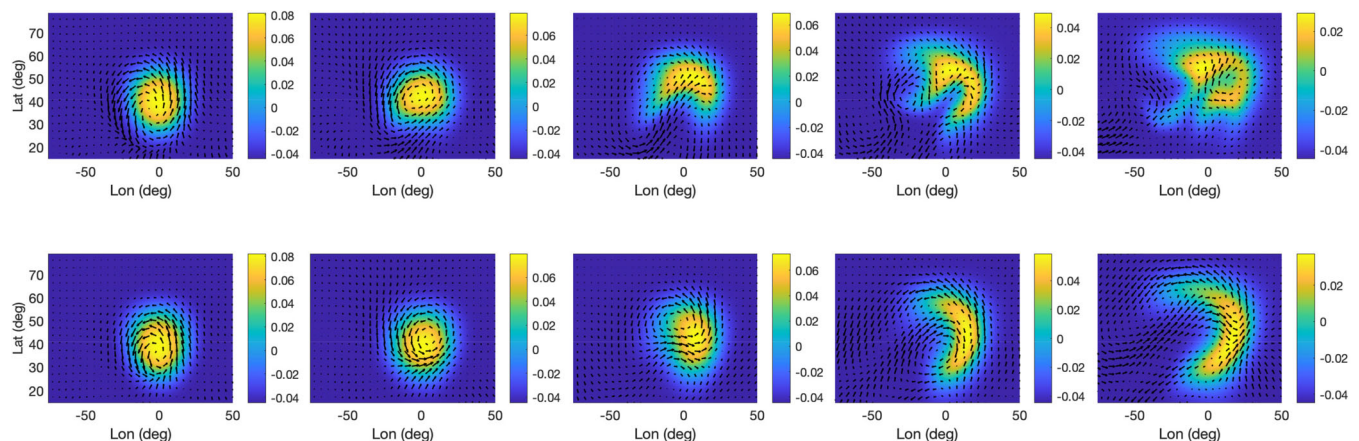


FIGURE 5 The evolution of buoyancy perturbations (represented in colors) in the lower layer and the corresponding velocity field (represented by arrows) during midlatitude adjustment in “dry” environment. The top and bottom rows show the results for barotropic and baroclinic configurations, respectively. The panels in each row display the evolution of the fields at 6, 13, 26, 43, and 65 days after the start of the simulation, arranged from left to right.

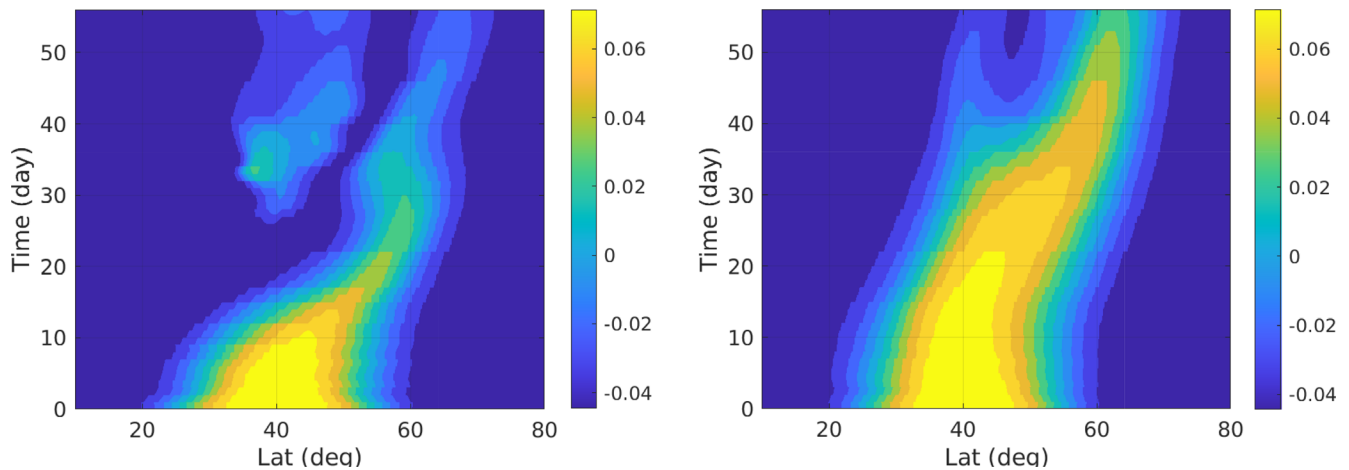


FIGURE 6 Hovmöller diagrams were employed to visualize the spatiotemporal evolution of buoyancy anomalies in the lower layer under two distinct atmospheric configurations: barotropic (left panel) and baroclinic (right panel). In the baroclinic setup, characterized by a quiescent upper layer, the adjustment process takes place at midlatitudes, prompted by the introduction of a positive buoyancy anomaly in a moist-convective environment.

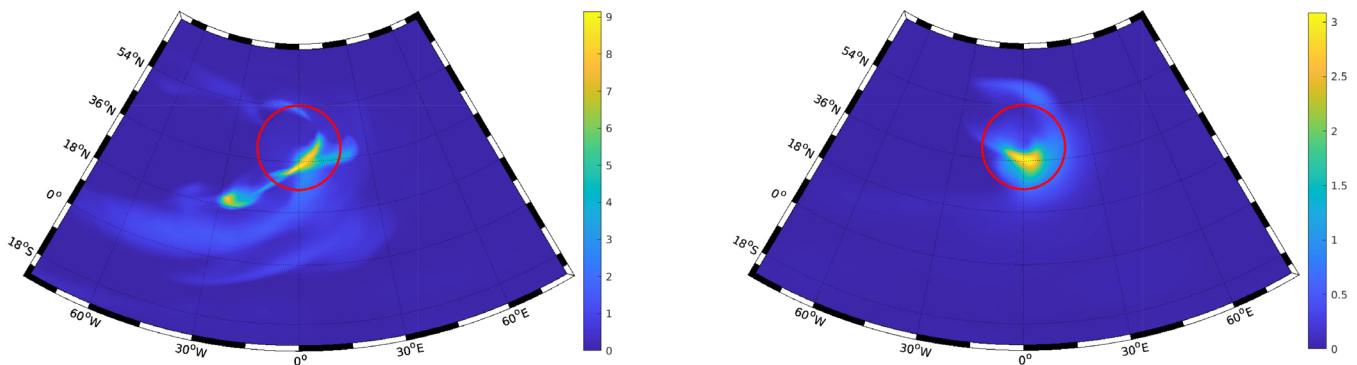


FIGURE 7 An asymmetric distribution of integrated CLWC was observed over 2 months for two different configurations: barotropic (left panel) and baroclinic (right panel). Both configurations were initialized with a strong buoyancy anomaly, with the red circle indicating the location of the large-scale, localized positive buoyancy anomaly at the initial time.

periphery of the anomaly, which can trigger the formation of small-scale vortices contributing to the heat transport.

Buoyancy forcing at mid-latitudes can trigger the formation of convective systems, which can lead to the formation of rain bands. Positive buoyancy anomalies in the lower troposphere over the ocean can arise from the warming of the ocean surface, subsequently influencing the lower atmosphere. The underlying causes of abrupt increases in SST encompass a range of factors, such as changes in the transport of heat by the ocean (Oliver et al., 2017; Pearce & Feng, 2013), including intensified boundary currents and reduced rates of heat loss from the ocean to the atmosphere, persistent large-scale atmospheric synoptic systems, and coupled air-sea feedback processes such as ENSO events (Bond et al., 2015; Lee et al., 2010; Rodrigues et al., 2019). This elevated

ocean surface temperature leads to the transfer of heat to the lower atmosphere through processes such as turbulent heat fluxes and sensible heat exchange (Perkins, 2015). This heating creates a thermal low-pressure system that can draw in moist air from surrounding regions. As the moist air rises, it can cool and form convective clouds that produce CLWC and precipitable water fronts. The resulting rain bands can bring relief to the high temperatures associated with heatwaves.

During the adjustment of a positive buoyancy anomaly, heatwaves can occur, leading to atmospheric instability and the formation of precipitation systems, such as rain bands. This instability arises from the release of free energy as latent heat during the process of moist convection, which is triggered by the presence of positive buoyancy anomalies. The resulting heating enhances instability and promotes further convection, leading to a positive feedback

loop. Figure 7 illustrates the formation of rain bands as the heatwave propagates. The distribution of total CLWC reveals an area of increased moist convection along the southern side of the buoyancy anomaly center. This leads to a westward veering of the Rossby wave group because the lower meridional modes move more quickly westward than the higher meridional modes. The nonuniform heating distribution from moist convection initiates pronounced Rossby wave group development, particularly in the barotropic configuration, which exhibits a northeast–southwest tilted distribution of total CLWC. This development results not only in the propagation of rain bands to the west but also in the formation of mesoscale convective systems. The adjustment process persists until the perturbation has dissipated, and the atmosphere has attained a state of enhanced stability. The spatial distribution of the integrated energy density anomaly in the lower layer (Figure 8) provides compelling evidence that the temporal evolution of the buoyancy anomaly in the lower troposphere is accompanied by the concurrent westward propagation of Rossby waves and the generation of inertia gravity waves, particularly in the southern sector of the buoyancy disturbance. These wave phenomena exhibit a more pronounced manifestation within the barotropic configuration compared to the baroclinic configuration. As Rossby waves propagate and interact with the buoyancy anomaly, they can enhance or deplete the energy density depending on their phase and intensity. For example, regions, where Rossby waves reinforce the buoyancy anomaly, can exhibit higher energy density, while regions where Rossby waves counteract or disrupt the buoyancy anomaly may display lower energy density.

4 | CONCLUSIONS

The nonlinear evolution of a large-scale localized positive buoyancy anomaly at mid-latitudes and the corresponding condensation patterns within a complete sphere were investigated using an idealized two-layer TRSW model in both “dry” and moist-convective environments, encompassing barotropic and baroclinic configurations. Our study yielded some insights into the intricate dynamics and thermodynamic processes associated with the development and propagation of buoyancy anomalies. The results show that intense buoyancy anomalies emerge as fundamental drivers in the initiation of cyclonic structures characterized by thermal lows in the lower troposphere. These structures act as catalysts for the subsequent formation of upper-tropospheric anticyclonic structures. This highlights the significance of atmospheric ridges in the middle to upper troposphere as potential superior predictors of surface warm extremes, surpassing the predictive capacity of surface anticyclones. During the early stages of positive buoyancy anomaly adjustment, a nearly isotropic inflow towards the center of the anomaly is observed, exerting an attractive force on surrounding air masses from all directions. This initial isotropic flow pattern lays the foundation for subsequent asymmetrical flow patterns. As the buoyancy anomaly evolves, the Coriolis force begins to influence the wind direction, causing deviations from the center. This leads to the development of distinct asymmetric convergent zones where air masses converge towards the center of the anomaly from specific directions. The emergence of these asymmetrical flow patterns alters the large-scale

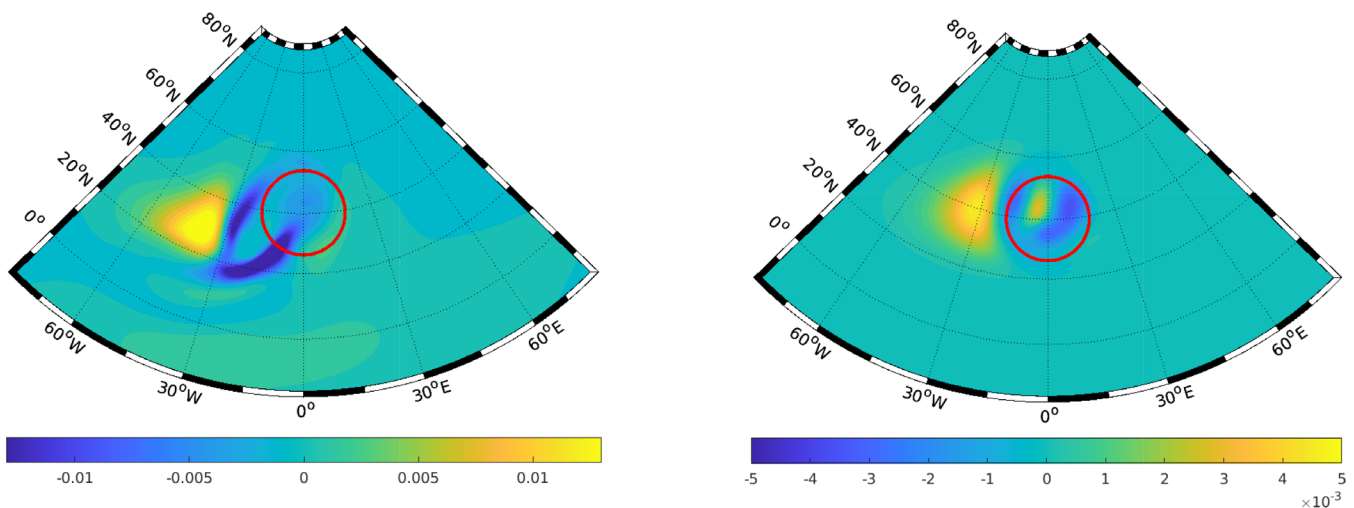


FIGURE 8 An asymmetric spatial distribution of the integrated energy density anomaly in the lower layer within a moist-convective environment was observed over a monthly duration for two distinct configurations: barotropic (left panel) and baroclinic (right panel). In both configurations, a strong buoyancy anomaly was utilized, and the initial temporal snapshot is denoted by the red circle, signifying the location of the large-scale, localized positive buoyancy anomaly.

circulation, imparting perturbations that can influence the development and evolution of other weather systems within the region.

In addition to their impact on local weather patterns, our findings indicate that buoyancy anomalies also contribute to the formation of mesoscale convective systems triggered by heatwaves in a moist-convective environment. These convective systems can generate heavy rainfall and rain bands, particularly in the southern and western sectors adjacent to the buoyancy anomaly. Inertia-gravity waves play a vital role in the redistribution of heat and momentum within the lower troposphere, with their emission occurring during the initial stages of midlatitude adjustment. These waves contribute to the complex dynamics of the system, influencing the transport and distribution of energy within the atmosphere. The evolution of precipitable water in the upper troposphere is a significant factor in the overall behavior of the system, resulting in the formation of a characteristic comma cloud pattern. This pattern serves as a visible manifestation of the intricate interplay between moisture dynamics and buoyancy anomalies.

Comparing the barotropic and baroclinic configurations, it is observed that inertia-gravity wave activity is more pronounced in the barotropic configuration than that of baroclinic when coupled with a stagnant upper layer. This highlights the sensitivity of wave behavior to the specific atmospheric conditions and configuration. Both weak and strong buoyancy anomalies exhibit a characteristic comma-shaped structure and are propelled northwestward by the beta-gyres. This northwestward motion contributes to the transport of heat and energy, influencing the regional climate dynamics. During the late stages of strong buoyancy anomaly evolution, particularly in barotropic configurations, a breaking process occurs. This breaking process can lead to the transport of a parallel heat flux toward the north, contributing to the redistribution of energy within the system. Buoyancy forcing at mid-latitudes acts as a triggering mechanism for the formation of convective systems, which in turn can give rise to the formation of rain bands. These rain bands contribute to the regional precipitation patterns and play a role in shaping the overall weather conditions.

Given the conceptual nature of this study, it is imperative to acknowledge the absence of certain factors, namely, the background gradient of potential temperature, zonal velocity, radiative transfer, and topography. These elements will be the subject of investigation in future studies employing Aeolus 2.0, an atmospheric model renowned for its intermediate complexity. It is noteworthy that the mcTRSW model serves as the dynamic core within the Aeolus 2.0 framework. By incorporating these aforementioned factors into subsequent

research endeavors, our objective is to attain a more comprehensive and realistic understanding of their intricate influences on the dynamics and behavior of the atmospheric system.

AUTHOR CONTRIBUTIONS

Masoud Rostami: Conceptualization; data curation; formal analysis; funding acquisition; investigation; methodology; project administration; resources; software; supervision; validation; visualization; writing – original draft. **Luca Severino:** Data curation; investigation; software; validation; visualization. **Stefan Petri:** Conceptualization; data curation; investigation; methodology; resources; software; visualization. **Saeed Hariri:** Investigation; methodology; resources; software; validation.

ACKNOWLEDGMENTS

We are grateful to Stefan Rahmstorf and Georg Feulner for stimulating discussions. This research was partially funded by the H&M Foundation (project number 20A048). Open Access funding enabled and organized by Projekt DEAL.

CONFLICT OF INTEREST STATEMENT

The authors report no conflict of interest.

ORCID

Masoud Rostami  <https://orcid.org/0000-0003-1730-5145>
Stefan Petri  <https://orcid.org/0000-0002-4379-4643>

REFERENCES

- Betts, A. & Miller, M. (1986) A new convective adjustment scheme. Part II: single columns tests using GATE wave, BOMEX, ATEX and arctic air-mass data sets. *Quarterly Journal of the Royal Meteorological Society*, 112, 693–762.
- Black, E., Blackburn, M., Harrison, G., Hoskins, B. & Methven, J. (2004) Factors contributing to the summer 2003 European heatwave. *Weather*, 59, 217–223. Available from: <https://doi.org/10.1256/wea74.04>
- Blumen, W. (1972) Geostrophic adjustment. *Reviews of Geophysics*, 10, 485–528.
- Bond, N.A., Cronin, M.F., Freeland, H. & Mantua, N. (2015) Causes and impacts of the 2014 warm anomaly in the NE Pacific. *Geophysical Research Letters*, 42, 3414–3420. Available from: <https://doi.org/10.1002/2015GL063306>
- Bouchut, F., Lambaerts, J., Lapeyre, G. & Zeitlin, V. (2009) Fronts and nonlinear waves in a simplified shallow-water model of the atmosphere with moisture and convection. *Physics of Fluids*, 21, 116604. Available from: <https://doi.org/10.1063/1.3265970>
- Carlson, T.N. (1980) Airflow through midlatitude cyclones and the comma cloud pattern. *Monthly Weather Review*, 108, 1498–1509 https://journals.ametsoc.org/view/journals/mwre/108/10/1520-0493_1980_108_1498_atmcat_2_0_co_2.xml
- Cassou, C., Terray, L. & Phillips, A.S. (2005) Tropical Atlantic influence on European heat waves. *Journal of Climate*, 18,

- 2805–2811 <https://journals.ametsoc.org/view/journals/clim/18/15/jcli3506.1.xml>
- Chang, M., Ho, C.-H., Chan, J.C.L., Park, M.-S., Son, S.-W. & Kim, J. (2019) The tropical transition in the Western North Pacific: the case of tropical cyclone Peipah (2007). *Journal of Geophysical Research – Atmospheres*, 124, 5151–5165. Available from: <https://doi.org/10.1029/2018JD029446>
- Diffenbaugh, N.S. & Ashfaq, M. (2010) Intensification of hot extremes in the United States. *Geophysical Research Letters*, 37, L15701. Available from: <https://doi.org/10.1029/2010GL043888>
- Fischer, E.M., Seneviratne, S.I., Vidale, P.L., Lüthi, D. & Schär, C. (2007) Soil moisture–atmosphere interactions during the 2003 European summer heat wave. *Journal of Climate*, 20, 5081–5099 <https://journals.ametsoc.org/view/journals/clim/20/20/jcli4288.1.xml>
- Gill, A. (1982) Studies of moisture effects in simple atmospheric models: the stable case. *Geophysical and Astrophysical Fluid Dynamics*, 19, 119–152. Available from: <https://doi.org/10.1080/03091928208208950>
- Gill, A.E. (1976) Adjustment under gravity in a rotating channel. *Journal of Fluid Mechanics*, 77, 603–621.
- Hansen, J., Sato, M. & Ruedy, R. (2012) Perception of climate change. *Proceedings of the National Academy of Sciences of the United States of America*, 109, E2415–E2423. Available from: <https://doi.org/10.1073/pnas.1205276109>
- Holton, J. (2004) *An introduction to dynamic meteorology*. Washington: Elsevier.
- Horton, R.M., Mankin, J.S., Lesk, C., Coffel, E. & Raymond, C. (2016) A review of recent advances in research on extreme heat events. *Current Climate Change Reports*, 2, 242–259. Available from: <https://doi.org/10.1007/s40641-016-0042-x>
- Katsaros, K. (2001) Evaporation and humidity. In: Steele, J.H. (Ed.) *Encyclopedia of ocean sciences*. Oxford: Academic Press, pp. 870–877 <http://www.sciencedirect.com/science/article/pii/B012227430X000684>
- Kossin, J.P., McNoldy, B.D. & Schubert, W.H. (2002) Vortical swirls in hurricane eye clouds. *Monthly Weather Review*, 130, 3144–3149 https://journals.ametsoc.org/view/journals/mwre/130/12/1520-0493_2002_130_3144_vsihec_2.0.co_2.xml
- Lahaye, N. & Zeitlin, V. (2016) Understanding instabilities of tropical cyclones and their evolution with a moist convective rotating shallow-water model. *Journal of the Atmospheric Sciences*, 73, 505–523 <https://journals.ametsoc.org/view/journals/atsc/73/2/jas-d-15-0115.1.xml>
- Lambaerts, J., Lapeyre, G. & Zeitlin, V. (2011) Moist versus dry barotropic instability in a shallow-water model of the atmosphere with moist convection. *Journal of the Atmospheric Sciences*, 68, 1234–1252.
- Lambaerts, J., Lapeyre, G. & Zeitlin, V. (2012) Moist versus dry baroclinic instability in a simplified two-layer atmospheric model with condensation and latent heat release. *Journal of the Atmospheric Sciences*, 69, 1405–1426.
- Lambaerts, J., Lapeyre, G., Zeitlin, V. & Bouchut, F. (2011) Simplified two-layer models of precipitating atmosphere and their properties. *Physics of Fluids*, 23, 046603. Available from: <https://doi.org/10.1063/1.3582356>
- Lecoanet, D., Vasil, G.M., Burns, K.J., Brown, B.P. & Oishi, J.S. (2019) Tensor calculus in spherical coordinates using jacobi polynomials. Part–ii: implementation and examples. *Journal of Computational Physics*, 3, 100012 <https://www.sciencedirect.com/science/article/pii/S2590055219300289>
- Lee, T., Hobbs, W.R., Willis, J.K., Halkides, D., Fukumori, I., Armstrong, E.M. et al. (2010) Record warming in the South Pacific and western Antarctica associated with the strong Central-Pacific El Niño in 2009–10. *Geophysical Research Letters*, 37, L1970. Available from: <https://doi.org/10.1029/2010GL044865>
- Lim, H. & Chang, C.-P. (1981) A theory for midlatitude forcing of tropical motions during winter monsoons. *Journal of the Atmospheric Sciences*, 38, 2377–2392 https://journals.ametsoc.org/view/journals/atsc/38/11/1520-0469_1981_038_2377_atfmfo_2_0_co_2.xml
- Matsuda, Y. & Takayama, H. (1989) Evolution of disturbance and geostrophic adjustment on the sphere. *Journal of the Meteorological Society of Japan. Ser. II*, 67, 949–966. Available from: https://doi.org/10.2151/jmsj1965.67.6_949
- Meehl, G.A. & Tebaldi, C. (2004) More intense, more frequent, and longer lasting heat waves in the 21st century. *Science*, 305, 994–997. Available from: <https://doi.org/10.1126/science.1098704>
- Miralles, D.G., Gentile, P., Seneviratne, S.I. & Teuling, A.J. (2019) Land-atmospheric feedbacks during droughts and heatwaves: state of the science and current challenges. *Annals of the New York Academy of Sciences*, 1436, 19–35. Available from: <https://doi.org/10.1111/nyas.13912>
- Okajima, S., Nakamura, H. & Kaspi, Y. (2021) Cyclonic and anticyclonic contributions to atmospheric energetics. *Scientific Reports*, 11, 13202. Available from: <https://doi.org/10.1038/s41598-021-92548-7>
- Oliver, E.C.J., Benthuisen, J.A., Bindoff, N.L., Hobday, A.J., Holbrook, N.J., Mundy, C.N. et al. (2017) The unprecedented 2015/16 Tasman Sea marine heatwave. *Nature Communications*, 8, 16101. Available from: <https://doi.org/10.1038/ncomms16101>
- Pearce, A.F. & Feng, M. (2013) The rise and fall of the “marine heat wave” off Western Australia during the summer of 2010/2011. *Journal of Marine Systems*, 111–112, 139–156 <https://www.sciencedirect.com/science/article/pii/S0924796312002059>
- Perkins, S.E. (2015) A review on the scientific understanding of heatwaves—their measurement, driving mechanisms, and changes at the global scale. *Atmospheric Research*, 164–165, 242–267. <https://www.sciencedirect.com/science/article/pii/S0169809515001738>
- Perkins, S.E., Alexander, L.V. & Nairn, J.R. (2012) Increasing frequency, intensity and duration of observed global heatwaves and warm spells. *Geophysical Research Letters*, 39, L20714. Available from: <https://doi.org/10.1029/2012GL053361>
- Pfahl, S. & Wernli, H. (2012) Quantifying the relevance of atmospheric blocking for co-located temperature extremes in the Northern Hemisphere on (sub-)daily time scales. *Geophysical Research Letters*, 39, L12807. Available from: <https://doi.org/10.1029/2012GL052261>
- Ripa, P. (1993) Conservation laws for primitive equations models with inhomogeneous layers. *Geophysical & Astrophysical Fluid Dynamics*, 70, 85–111. Available from: <https://doi.org/10.1080/03091929308203588>
- Rodrigues, R.R., Taschetto, A.S., Sen Gupta, A. & Foltz, G.R. (2019) Common cause for severe droughts in South America and marine heatwaves in the South Atlantic. *Nature Geoscience*, 12, 620–626. Available from: <https://doi.org/10.1038/s41561-019-0393-8>

- Rostami, M. & Zeitlin, V. (2017) Influence of condensation and latent heat release upon barotropic and baroclinic instabilities of atmospheric vortices in a rotating shallow water model on the f-plane. *Geophysical & Astrophysical Fluid Dynamics*, 111, 1–31.
- Rostami, M. & Zeitlin, V. (2018) An improved moist-convective rotating shallow-water model and its application to instabilities of hurricane like vortices. *Quarterly Journal of the Royal Meteorological Society*, 144, 1450–1462. Available from: <https://doi.org/10.1002/qj.3292>
- Rostami, M. & Zeitlin, V. (2019a) Eastward-moving convection-enhanced modons in shallow water in the equatorial tangent plane. *Physics of Fluids*, 31, 021701.
- Rostami, M. & Zeitlin, V. (2019b) Geostrophic adjustment on the equatorial beta-plane revisited. *Physics of Fluids*, 31, 081702. Available from: <https://doi.org/10.1063/1.5110441>
- Rostami, M. & Zeitlin, V. (2020) Evolution, propagation and interactions with topography of hurricane-like vortices in a moist-convective rotating shallow-water model. *Journal of Fluid Mechanics*, 902, A24.
- Rostami, M. & Zeitlin, V. (2022a) Evolution of double-eye wall hurricanes and emergence of complex tripolar end states in moist-convective rotating shallow water model. *Physics of Fluids*, 34, 066602. Available from: <https://doi.org/10.1063/5.0096554>
- Rostami, M. & Zeitlin, V. (2022b) Instabilities of low-latitude easterly jets in the presence of moist convection and topography and related cyclogenesis, in a simple atmospheric model. *Geophysical & Astrophysical Fluid Dynamics*, 116, 56–77. Available from: <https://doi.org/10.1080/03091929.2021.1959574>
- Rostami, M., Zeitlin, V. & Spiga, A. (2017) On the dynamical nature of Saturn's north polar hexagon. *Icarus*, 297, 59–70 <https://www.sciencedirect.com/science/article/pii/S0019103516305978>
- Rostami, M., Zhao, B. & Petri, S. (2022) On the genesis and dynamics of madden-Julian oscillation-like structure formed by equatorial adjustment of localized heating. *Quarterly Journal of the Royal Meteorological Society*, 148, 3788–3813. Available from: <https://doi.org/10.1002/qj.4388>
- Sanders, F. & Gyakum, J.R. (1980) Synoptic-dynamic climatology of the “bomb”. *Monthly Weather Review*, 108, 1589–1606 https://journals.ametsoc.org/view/journals/mwre/108/10/1520-0493_1980_108_1589_sdcot_2_0_co_2.xml
- Stefanon, M., D'Andrea, F. & Drobinski, P. (2012) Heatwave classification over Europe and the Mediterranean region. *Environmental Research Letters*, 7, 014023. Available from: <https://doi.org/10.1088/1748-9326/7/1/014023>
- Thomson, S.I. & Vallis, G.K. (2018) Atmospheric response to SST anomalies. Part I: background-state dependence, teleconnections, and local effects in winter. *Journal of the Atmospheric Sciences*, 75, 4107–4124 <https://journals.ametsoc.org/view/journals/atsc/75/12/jas-d-17-0297.1.xml>
- Vasil, G.M., Lecoanet, D., Burns, K.J., Oishi, J.S. & Brown, B.P. (2019) Tensor calculus in spherical coordinates using Jacobi polynomials. Part-I: mathematical analysis and derivations. *Journal of Computational Physics*, 3, 100013 <https://www.sciencedirect.com/science/article/pii/S2590055219300290>
- White, R.H., Anderson, S., Booth, J.F., Braich, G., Draeger, C., Fei, C. et al. (2023) The unprecedented Pacific northwest heatwave of June 2021. *Nature Communications*, 14, 727. Available from: <https://doi.org/10.1038/s41467-023-36289-3>
- Xoplaki, E., González-Rouco, J.F., Luterbacher, J. & Wanner, H. (2003) Mediterranean summer air temperature variability and its connection to the large-scale atmospheric circulation and SSTs. *Climate Dynamics*, 20, 723–739. Available from: <https://doi.org/10.1007/s00382-003-0304-x>
- Zaitchik, B.F., Macalady, A.K., Bonneau, L.R. & Smith, R.B. (2006) Europe's 2003 heat wave: a satellite view of impacts and land-atmosphere feedbacks. *International Journal of Climatology*, 26, 743–769. Available from: <https://doi.org/10.1002/joc.1280>
- Zeitlin, V. (2018) *Geophysical fluid dynamics: understanding (almost) everything with rotating shallow water models*. Oxford: Oxford University Press.
- Zhou, G. (2019) Atmospheric response to sea surface temperature anomalies in the mid-latitude oceans: a brief review. *Atmosphere-Ocean*, 57, 319–328. Available from: <https://doi.org/10.1080/07055900.2019.1702499>

How to cite this article: Rostami, M., Severino, L., Petri, S., & Hariri, S. (2023). Dynamics of localized extreme heatwaves in the mid-latitude atmosphere: A conceptual examination. *Atmospheric Science Letters*, e1188. <https://doi.org/10.1002/asl.1188>